# Driven on- and off-lattice gas

Paul D. Siders
*Department of Chemistry and Biochemistry, University of Minnesota Duluth, Duluth, Minnesota 55812, USA*
(Received 12 March 2009; published 1 June 2009)

An on- and off-lattice analog of the driven lattice gas has been studied by molecular-dynamics simulation. In the model, particles move on a two-dimensional lattice potential under a constant driving force. They also interact with each other by an attractive square-well pair potential. A heat bath removes as heat the work done by the driving field. The case of zero field recovers equilibrium two-dimensional lattice and continuous-space results. With nonzero field and a strong lattice potential, the system is comparable to the driven lattice gas. As in the driven lattice gas, the anisotropic single-strip configuration persists to higher kinetic energy as the field strength increases. In the case of zero lattice strength, the model reduces to an off-lattice two-dimensional driven square-well fluid. Single-strip steady states are not observed off lattice.

DOI: 10.1103/PhysRevE.79.061101 PACS number(s): 05.70.Ln, 05.10.−a, 64.60.De, 64.75.Gh

## I. INTRODUCTION

The driven lattice gas (DLG) is a fundamental model in nonequilibrium statistical mechanics. The model consists of atoms distributed on a square lattice, each atom subjected to a constant force parallel to one of the lattice vectors. Below a critical temperature, an anisotropic phase appears in which atoms separate into a low-density gas and a high-density high-conductivity strip parallel to the driving field. The critical temperature for phase separation rises with increasing field strength.

This work introduces a two-dimensional molecular-dynamics (MD) model in which particles are driven either on an underlying square-lattice potential or off the lattice, on a smooth plane. The driven particles are referred to as "atoms" in this work. Atoms driven upon a square lattice form a single-strip phase similar to that seen in the DLG and that phase persists to higher kinetic energies when the field strength is greater. When the lattice potential is removed, no single-strip phase forms.

Adding a periodic external potential to an equilibrium molecular-dynamics calculation has been done before. Strepp *et al.* [1,2] studied the phase diagram of hard and soft particles moving in two dimensions under the influence of a periodic potential. Chaudhuri *et al.* [3] observed freezing and re-entrant melting due to a periodic potential acting on attractive disks in two dimensions. It is recognized that a lattice potential added to a planar system may alter fluid and solid states and introduce new phases, especially if the potential is incommensurate with the system's unconstrained solid state.

Colloidal particles in an external potential such as that due to an optical-tweezers array [4] have been modeled by Potiguar and Dickman [5] with Monte Carlo methods. In their work, particles moved on a smooth potential [6] having a square array of deep wells. Particles interacted with a continuous pair potential, out to third-nearest neighbors. A weak driving field raised the melting temperature, as happens in the DLG, but then greater field strength depressed the melting temperature.

Fully off-lattice analogs of the DLG have been studied before. Marro *et al.* [7,8] devised an off-lattice driven Lennard-Jones fluid (DLJF) and studied it by Monte Carlo simulation. They observed an anisotropic driven phase and found that the critical temperature for its disappearance *declined* with increasing field strength. Declining critical temperature was related to increased freedom in the hopping direction, off lattice. Díez-Minguito *et al.* [9] concluded that "the DLG does not have a simple off-lattice analog. This is because the ordering agent in the DLG is more the lattice geometry than the field itself."

Another indication that the underlying square lattice is necessary to the original DLG's behavior comes from Monte Carlo simulation of the DLG on triangular and hexagonal lattices. Varying lattice connectivity and field orientation relative to the lattice altered DLG properties: weakening and broadening the transition to an anisotropic phase [10]. An anisotropic phase was observed only for special relative orientations of field and lattice. The present work will move a driven gas off of its lattice to compare the nature of the phases observed on and off of an underlying lattice potential.

The DLG was originally studied by Monte Carlo methods [11,12]. It has also been studied by mean-field methods [13–16], Langevin-equation and field-theoretic methods [17–22], and by high-temperature expansion [23]. Also, its Markov master equation has been solved exactly for steady states on half-filled small lattices [10,24–26]. In this work, dynamics will be calculated directly by hard-particle MD simulation, a method not previously applied to the DLG. The MD method naturally suits driven particles especially off lattice. However, the limit of an infinitely strong driving field, a limit often studied for the DLG, is not accessible in MD because such a field would accelerate particles infinitely. This work addresses only finite field strength.

## II. METHODS

### A. Pair potential

The square-well potential was chosen because it is simple and it closely mimics lattice-gas pair interactions. The lattice-gas potential may be described in terms of $r$, the distance between two gas atoms, and $L$, the lattice's nearest-neighbor site-site distance. The lattice-gas potential is infinite

 

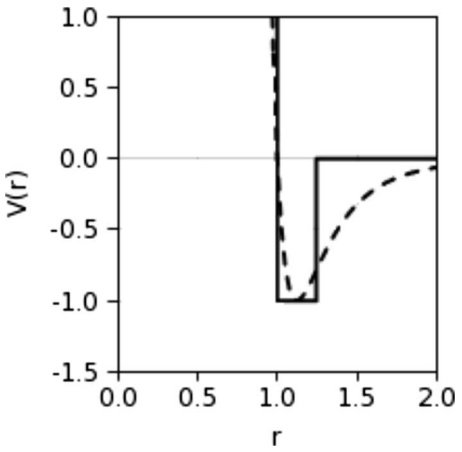


FIG. 1. The square-well potential (solid) and the Lennard-Jones potential (dashed). $V$ is in units of $\epsilon$; $r$ is in units of $\sigma$.

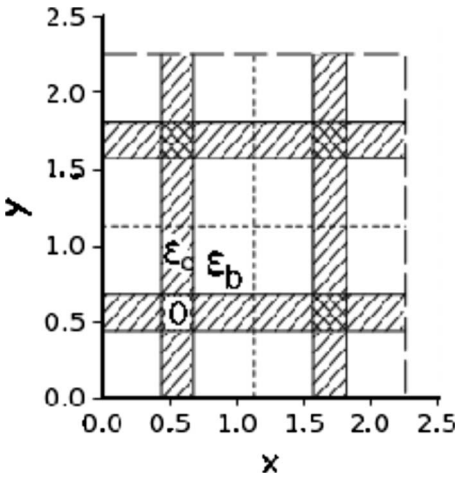


FIG. 2. A cell (four unit cells) of the lattice potential. Lattice sites have potential energy zero. Channel and barrier potential energies are $\epsilon_c$ and $\epsilon_b$. Coordinates are in units of the hard-core diameter, $\sigma$.

for $r<L$ (preventing multiple occupancy of any site), equals $-\epsilon$ for $r=L$ (i.e., for nearest-neighbor atoms), and is zero for $r>L$ (i.e., for all sites beyond nearest neighbors).

In this work, well depth, $\epsilon$, is the unit of energy. As customary, the square-well potential's hard-core diameter, $\sigma$, is the unit of length. Time has units of $\sigma(m/\epsilon)^{1/2}$ [27], but because atomic mass $m$ is unspecified, time will be left unitless. The attractive range of the square well (denoted "$c$" by Young and Alder [28], $\lambda$ by Kiselev *et al.* [29] and by Singh and Kwak [30], "$b$" by Skibinsky *et al.* [31], "$(1+\delta/\sigma)$" by Bolhuis *et al.* [32], for example) affects the phase diagram and viscosity [33] of equilibrium square-well fluids. For this work, the range $c$ was chosen to make the attractive well resemble the attractive part of a Lennard-Jones potential having the same $\sigma$. The value $c=(2^{7/6}-1)=1.2449\ldots$ matches the square-well and Lennard-Jones potentials at zero potential and at the center of the square attractive well, as shown in Fig. 1.

In summary, the square-well potential used in this work is

$$V(r)=\begin{cases}\infty; r<1\\ -\epsilon; 1<r<2^{7/6}-1\\ 0; r>2^{7/6}-1\end{cases}. \quad (1)$$

With zero driving force and a weak lattice, the present model reduces to the equilibrium square-well fluid in two dimensions. There is a solid phase at low temperature. Because the attractive range of the potential is small, the only solid expected is hexagonal close packed [28,29,31]. Because the lattice potential's attractive region is flat, nonzero lattice strength may lead to an incommensurate solid at low temperature, but the lowest-energy calculations reported here do not show a hexagonal crystal on the lattice potential. Rather, the lowest temperatures reached (under zero driving force) with the present method yielded a mixture of hexagonally packed and registered solid regions.

### B. Lattice potential

Molecular dynamics on a normal lattice, which has point sites connected by one-dimensional paths, would be difficult. The present work uses a two-dimensional array of site, channel, and barrier potentials to influence atom dynamics, guiding atoms to latticelike movement without restraining the atoms to a lattice of lower dimension. One four-site cell of the lattice potential is shown in Fig. 2. The center of each site is analogous to a site or vertex on a square lattice. Channels are analogous to lattice connections or edges.

Distances are in units of the hard-core diameter. Four sites in each cell have zero potential energy. Barriers have potential $\epsilon_b$. Channels between sites have positive potential $\epsilon_c$, where $\epsilon_c<\epsilon_b$. At low kinetic energy, the lattice potential influences atoms to occupy lattice sites and follow channels between sites. At the lowest kinetic energies, the atoms may freeze onto lattice sites or may form an incommensurate solid. At high kinetic energy the underlying lattice potential has little effect.

The site-site distance, center to center, was set to 1.13. That distance was chosen because it is approximately the average atom-atom separation at the critical density for a melting hard-disk solid.

Each barrier has side length 0.89. That distance was chosen so that the barrier's diagonal slightly exceeds the range of attractive interactions, $(2^{7/6}-1)$, preventing attractive interactions ("bonds") between atoms located in next-nearest-neighbor sites. Such should be prevented because the simple lattice gas and the DLG have nearest-neighbor attractions only, not next-nearest-neighbor attractions. The width of channels and sites is $1.13-0.89=0.24$.

The channel and barrier potentials were set to $\epsilon_c=0.5$ and $\epsilon_b=3.0$, in units of the attractive well depth $\epsilon$. The lattice potential strength is scaled with a parameter $\lambda; 0\leq\lambda\leq 1$. As the lattice potential strength is varied, the system passes from an off-lattice two-dimensional square-well fluid to a continuous analog of the lattice gas.

Atoms move according to classical mechanics, subject to impulsive interactions with each other, and subject to a constant force $F$. In the present work, the driving force is in the $x$ direction.

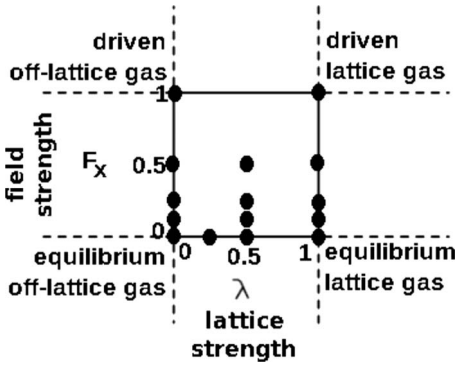


FIG. 3. Scheme for varying lattice and field strengths. Filled circles represent $(F_x,\lambda)$ pair for which molecular-dynamics data were collected.

Figure 3 shows schematically the $(F_x,\lambda)$ space and four limiting cases. Those cases and passages between them are examined in this work.

Periodic toroidal boundary conditions allow a net particle current in the $x$ direction. Data are reported for runs using 1152 atoms on a $24\times24$, 2304-site lattice. That half-filling corresponds to the lattice gas's critical density, $\rho=0.5$ atom per site.

Methods used to study the driven lattice gas and the related driven Lennard-Jones fluid have included Monte Carlo simulation, kinetic mean-field theory, and exact analyses of Markov-chain transition matrices. The most extensive analyses of large systems have been Monte Carlo simulations. Molecular dynamics has not been applied to the driven lattice gas, even though molecular dynamics has some advantages for nonequilibrium problems: (i) time appears, rather than number of Monte Carlo steps, a proxy for time. The explicit time in molecular dynamics allows study of relaxation toward steady states. (ii) Choice of a rate function (e.g., Metropolis, Glauber), which affects the nature and coexistence of steady states [34], is avoided. (iii) Temperature does not appear. In the DLG, particles at lattice sites equilibrate with the heat bath, the temperature of which enters Monte Carlo hopping rates. In nonequilibrium molecular dynamics, temperature is not simply defined. Methods for calculating temperature in nonequilibrium dynamics were discussed by Casas-Vazquez and Jou [35], Morriss and Rondini [36], Baranyai [37,38], Jepps *et al.* [39], and Hoover and Hoover [40]. In this work, the computationally simplest method has been adopted: average kinetic energy per atom in two dimensions, $E_{kin}$, stands for temperature. It may not be an entirely satisfactory stand-in for temperature. For example, kinetic energy may be both inhomogeneous and anisotropic.

### C. Heat bath

A heat bath is applied because work done by the driving field must be removed to prevent runaway acceleration of the atoms. Heat removal is essential to driven dynamics. The choice of heat bath is important. In a nonequilibrium system, the nature of the heat bath and the way it is coupled to the system contribute to properties of even the steady states of the system [41].

A heat bath for the present step-potential molecular dynamics should not alter the equations of motion because that would reduce the computational benefits of impulsive dynamics. Also, for the present model, the bath should not require that the system has a temperature because of the difficulty defining such. For those reasons, the Hoover and Nosé thermostats [42] are not optimal for the present model. The Gaussian thermostat defined by Todd and Daivis [43] is attractive but requires calculation of the streaming velocity. To place streaming or peculiar velocities near the heart of the simulation would be bad because it is anticipated that the present model will, under some conditions, develop inhomogeneous velocity distributions. Whatever heat bath is used, it must be of the "profile-unbiased" type, because velocity-profile assumptions in thermostats have caused spurious along-field ordering in other systems [44,45]. Another class of thermometers, configurational thermometers and thermostats [44], are ill-suited to the step potentials of this work.

For this work, the heat bath adopted is simple, controls acceleration due to work done by the field, and does not modify particle trajectories between collisions. It requires neither local temperature nor peculiar velocity. The heat bath defined for the present system simply conserves total energy by extracting kinetic energy at a rate equal, averaged over time, to the rate at which the field does work. Let $J$ be the rate at which the bath adds energy as heat, by scaling atom kinetic energies. Typically, $J$ is negative. The bath's heat rate, $J$, evolves according to the following equations:

$$\frac{d(\Delta U)}{dt} = J + \frac{dW}{dt}, \tag{2}$$

$$\frac{dJ}{dt} = -\frac{\Delta U(t)}{\tau^2} - \frac{2}{\tau}\left(J + \frac{dW}{dt}\right). \tag{3}$$

In Eqs. (2) and (3), $W$ is work done by the field and $\frac{dW}{dt}$ is the rate at which the field does work on the atoms. The energy difference $\Delta U$ is cumulative over the molecular-dynamics run, the sum of work done by the field and heat supplied (negative) by the bath. The first equation represents conservation of energy. The two equations may be combined to give a second-order differential equation for $J$, that equation being formally the equation of a damped driven oscillator. Based on that analogy, $\tau$ is the inverse of the natural undriven frequency for $J$. The initial value of $J$ is taken to be $L(N/E_{kin})^{1/2}$, where $L$ is the site-to-site distance (1.13) and $E_{kin}$ is the kinetic energy of the $N$-atom configuration.

During a molecular-dynamics run, the heat bath $J$ is applied to atoms at lattice-potential boundaries, so $-J$ represents heat extracted by the lattice from kinetic energy of atoms. At every atom-lattice collision, both $x$ and $y$ components of the atom's velocity are scaled by $(1+\frac{J\Delta t}{E_{kin}})^{1/2}$, where $\Delta t$ is the time since the last atom-lattice collision and $E_{kin}$ is the kinetic energy (of the $N$-atom system).

As steady state is approached, $dW/dt$ becomes approximately constant. Then $J$ approaches $-dW/dt$ and $\Delta U$ also becomes constant. In the absence of fluctuations and numerical error, $\Delta U=0$. In fact, $J$ and $dW/dt$ nearly cancel but $\Delta U$ will fluctuate and may not precisely average to zero. The

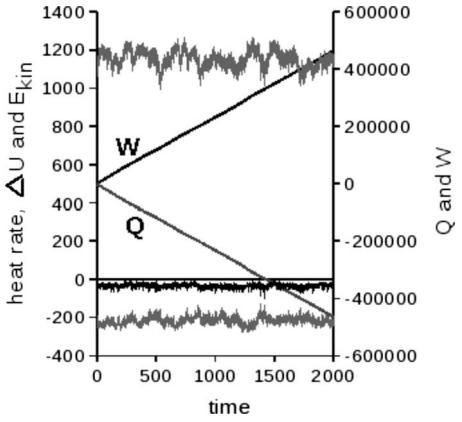


FIG. 4. Sample behavior of the heat bath for the gas driven upon a lattice. $F_x=1$, $\lambda=1$, and $N=1152$. At $t=1000$, from the bottom of the figure to the top, are graphed $J$, $\Delta U$, $Q$, $W$, and $E_{kin}$. The average $E_{kin}$ is 1159, or 1.01 per atom. Energy, heat, and work are in units of $\epsilon$, the pair potential's well depth. Time is unitless.

heat rate is calculated from discrete-time atom-lattice collisions, as explained above. The work rate may be calculated in two ways. At any particular time, $\frac{dW}{dt}=\Sigma F\cdot v_i$, where $v_i$ is the velocity of the $i$th atom. Because $F$ is directed in the $x$ direction, and all atoms have the same and unit mass, this instantaneous $\frac{dW}{dt}$ is simply the magnitude of the force times the total velocity in the $x$ direction. Another method for calculating $\frac{dW}{dt}$ uses the recorded $W(t)$, the cumulative work done by the field during the simulation. $W(t)=\Sigma F_j\Delta x_j$, where $\Delta x_j$ is the $x$ displacement of an atom during event $j$, and the sum runs over all displacements of all atoms, up to time $t$. Likewise, a cumulative heat $Q(t)=\Sigma J_m(\Delta E_{kin})_m$, where the sum is over all atom-lattice collisions up to time $t$. One expects to find $\Delta U(t)=Q(t)+W(t)$ at all times, allowing for fluctuations and a time lag between work and heat.

Applying the bath at lattice potential boundaries has the consequence that although work is performed continuously, heat is extracted at intervals. It is possible for work to be done more rapidly in atoms' flights between potential boundaries than the bath can remove it at boundaries. In practice, this has been a problem only when the lattice potential is flat ($\lambda=0$), average kinetic energy is low, and of course $F_x$ is nonzero. Under those conditions, atoms have a streaming velocity and $\frac{dW}{dt}=\Sigma F_x v_{x,i}$ is large.

The simulations reported in this work calculated $\frac{dW}{dt}$ in the $\frac{dJ}{dt}$ equation from instantaneous work (i.e., from total $x$ velocity). The derivative $\frac{dJ}{dt}$ was integrated by simple rectangular integration as the simulation ran. Figure 4 shows $W$, $\Delta U$, $Q$, and $J$ during 2000 time units of a typical run. The $N$-atom configuration's kinetic energy is also shown in Fig. 4. For the run shown, $\lambda=1$ and $F_x=1$. The figure shows that heat rate $J\approx-200$ kept $\Delta U$ nearly constant and near zero, compensated for the work done by the field and allowed the configuration's kinetic energy to fluctuate around a steady value. In Fig. 4, the left-hand ordinate is for $J$, $\Delta U$, and total kinetic energy. The right-hand vertical axis is for $Q(t)$ and $W(t)$.

Although it might have been possible to define local anisotropic temperature in terms of peculiar velocity relative to streaming velocity, that approach was not taken. In such an approach, the position-dependent streaming velocity would have to be known or quickly estimated in order to establish the heat bath, and once established the bath would favor retention of the initial assumption or estimate. Although streaming velocity could be calculated more efficiently if a velocity profile could be assumed, an assumed profile may tend to enhance ordering along the field [43]. Calculating the streaming velocity adaptively by mere binning might avoid biasing steady-state results, but would require long runs, especially to acquire good data in low-density regions. *After* steady state has been reached, streaming velocity can be calculated by binning. Indeed, the current density graphed in Sec. II G is proportional to binned streaming velocity.

Peculiar velocity and the related local temperature were calculated for off-lattice dynamics, see Sec. III B and Fig. 13, to estimate local temperature. The calculation was possible because off-lattice, streaming velocity was approximately homogeneous. Inhomogeneous single-strip phases prohibited such a temperature calculation for on-lattice dynamics.

### D. Collision dynamics

As usual in hard-potential dynamics, equations of motion were easily integrated between events. The time to reach a lattice-potential boundary was easily calculated as the root of a quadratic equation. For any given atom, the time to its next collision with another atom was also readily calculated. In the absence of a driving field, exact collision dynamics was given by Rapaport [46] and by Alder and Wainright [47]. Because the time to collision is unaffected by the driving force, so long as both atoms move under the same driving force, those solutions apply in the present work as well. A special case occurs when an atom is pinned by the driving field against a step of the lattice potential preventing its acceleration by the field. In that case time to collision with a freely moving atom is the root of a quartic equation, and roots were calculated numerically.

### E. Event tree

Calculations were organized in a binary tree of events. An event is an atom-atom collision, an atom reaching a potential or cell boundary, a heat-bath update, or a nondynamic event such as data collection.

A typical computational run consisted of initial relaxation from $t=0$ to about $10^3$, followed by data collection over 1000 to 2000 time units. In time increment $\Delta t=1$, approximately 10 to 100 events occurred per atom, so data collection occurred over $10^7-10^8$ events. In their Monte Carlo simulation of an off-lattice Lennard-Jones fluid Marro *et al.* [7] calculated steady-state properties from $10^6$ configurations. For comparison, steady-state molecular-dynamics averages in this work reflect approximately $10^4-10^5$ events per atom. Multiple runs were necessary to reach steady state. Relaxation to a steady state was slow at low kinetic energies and near transitions. Spatial reorganization within a high-density strip was exceedingly slow, perhaps because little kinetic energy was available within the strip.

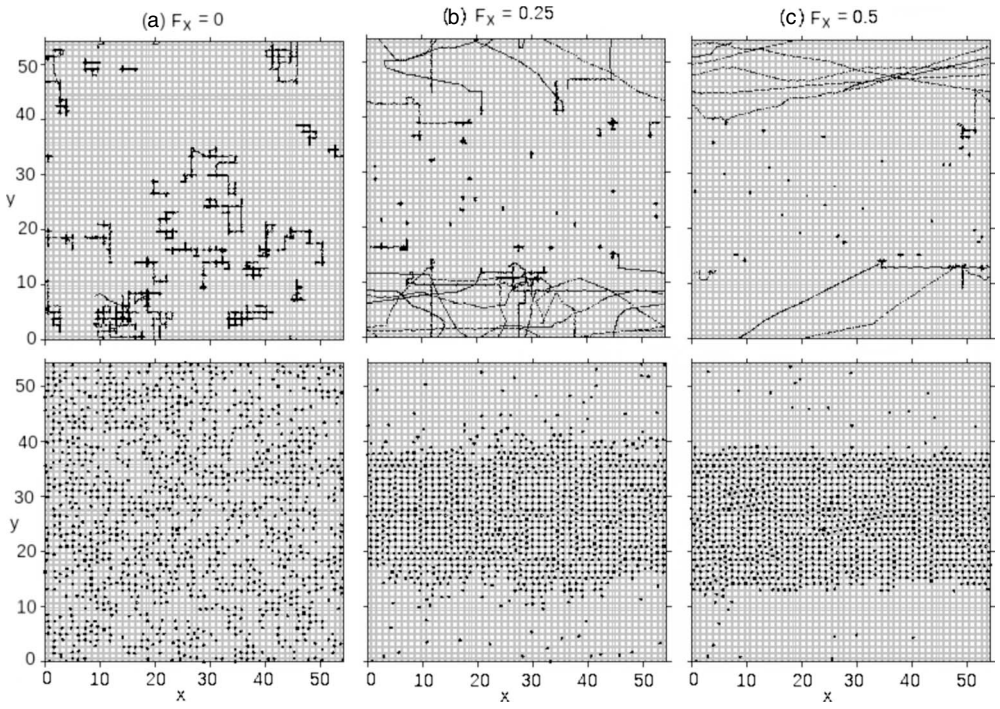


FIG. 5. $\lambda=1$ and $E_{kin}=0.7$ The upper figures show trajectories of 32 atoms for 200 time units. The lower figures show the locations of all 1152 atoms at one time. (a) $F_x=0$. (b) $F_x=0.25$. (c) $F_x=0.5$. Coordinates $x$ and $y$ are in units of $\sigma$; force is in units of $\epsilon/\sigma$.

### F. Configurations and trajectories

An $N$-atom configuration consists of all atoms' positions and velocities. Although each atom had its own local time during a simulation, all atoms were updated to a common time before configurations were used for property collection. Figure 5 shows typical trajectories superimposed on the lattice potential and snapshot configurations.

Shown are trajectories for 32 of the 1152 atoms moving upon a $24\times24$ lattice for 200 time units. Configurations were drawn from the same simulations runs as the trajectories but show all 1152 atoms at a single common time. All three of Figs. 5(a)–5(c) correspond to approximately the same average kinetic energy, 0.7 (per atom, in units of $\epsilon$). The driving field $F_x$ is zero for Fig. 5(a), 0.25 for Fig. 5(b), and 0.5 for Fig. 5(c). With zero driving field for Fig. 5(a), trajectories appear to be diffusive and resemble those of an equilibrium lattice gas, although these trajectories are continuous in two-dimensional space. Figure 5(a) shows a disordered and isotropic system, as expected because the driving field has zero strength and the kinetic energy (which equals temperature in this nondriven case) is above the freezing point, which is approximately 0.4. Raising the driving field to 0.25, Fig. 5(b), leads to a high-density single strip and makes velocity inhomogeneous and anisotropic. Atoms in the low-density regions have high velocities in the $x$ direction, accelerated by the field. In the high-density strip, atoms appear to be frozen into a registered solid. Doubling the field to $F_x=0.5$, Fig. 5(c), increases the velocity along the field direction in the low-density region without qualitatively altering the high-density strip.

When the lattice strength is zero and the field is also zero, the model reduces to the square-well fluid in two dimensions. Figure 6 shows 32 trajectories and an 1152-atom configuration with $\lambda=0$; no lattice potential. Comparable data for $\lambda=1$, the full lattice potential, are in Fig. 5(a). The configuration shown in Fig. 6 is similar to the configuration in Fig. 5(a), which is for the same temperature but has a nonzero lattice potential.

Describing the case $\lambda=0$ as lattice-free could be misleading. Although $\lambda=0$ does make zero the lattice's potential energy, the heat bath always operates upon atoms when they reach boundaries of the lattice potential, even in the limit of no change in potential at those boundaries. In the case $\lambda=0$, the lattice potential is flat but its boundaries are still used by the heat bath.

### G. Time-averaged properties

Time averages over an evolving configuration lead directly to kinetic, potential and total energy, the current, the number of bonds (where a "bond" is a pair of atoms separated by less than $c\sigma$), and the current density. Current density is the number of atoms per time per $\Delta y$ bin, leaving the simulation cell in the $x$ direction, periodically wrapping around to the left edge of the simulation region. In Fig. 7 there appears a local minimum in the current density at $E_{kin}\approx1.5$. The driven ($F_x=0.25$) energy flattens at the same kinetic energy. At the same kinetic energy, and for $F_x=0.25$ the structure factor perpendicular to the field goes to zero, and the high-density strip disappears, indicating a transition to an anisotropic and homogeneous phase.

Current density, density, and kinetic energy may vary along $y$ perpendicular to the field. These quantities were calculated as functions of $y$ by binning along $y$. Figure 8 shows the kinetic energy per atom in the $x$ and $y$ directions plotted

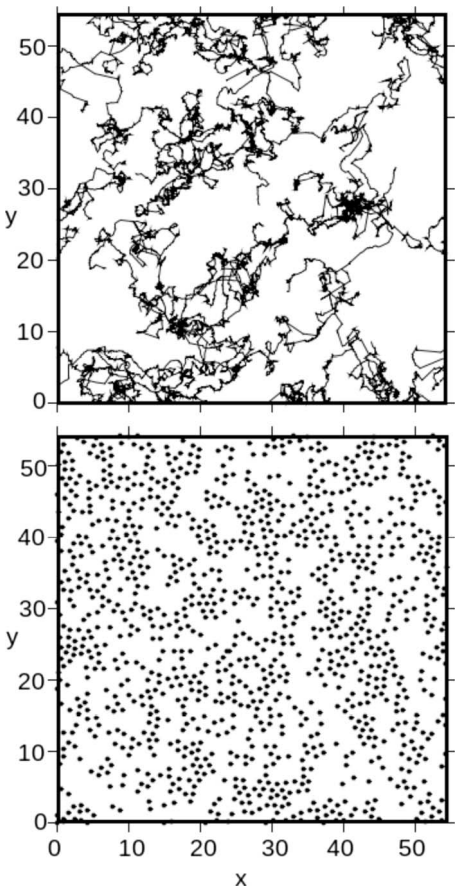


FIG. 6. $F_x=0$, $\lambda=0$ (off lattice), and $E_{kin}=0.7$. Upper: trajectories of 32 atoms over $\Delta t=200$. Lower: snapshot of one 1152-atom configuration. Coordinates $x$ and $y$ are in units of $\sigma$.

as functions of $y$. For reference, the particle density $\rho(y)$ is also graphed. In the central high-density strip, kinetic energy is low, isotropic, and approximately homogeneous ($E_{kin,x} \approx E_{kin,y}$, with little $y$ dependence). That is, the high-density strip appears to be a frozen cold slab of atoms. In the low-density region, kinetic energy is higher and anisotropic. Kinetic energy is higher along the field than perpendicular to the field. Even perpendicular to the field, the kinetic energy $E_{kin,y}$ is several times the equilibrium melting temperature, which is approximately 0.4. The overall steady state (for the particular conditions of Fig. 8) may be described as a cold slab coexisting with a hot low-density gas.

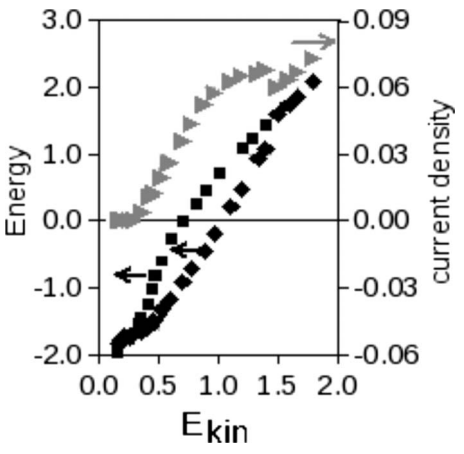


FIG. 7. Time-averaged energy and current density on a lattice, $\lambda=1$. On the abscissa is kinetic energy per particle. The middle data (squares) are at equilibrium ($F_x=0$). For the lower and upper data (diamonds and triangles), $F_x=0.25$. Total energy is on the left ordinate. Current density (top, triangles) is on the right ordinate. Energies are in units of $\epsilon$. The unit of current density unit is number of atoms per time per $\sigma$.

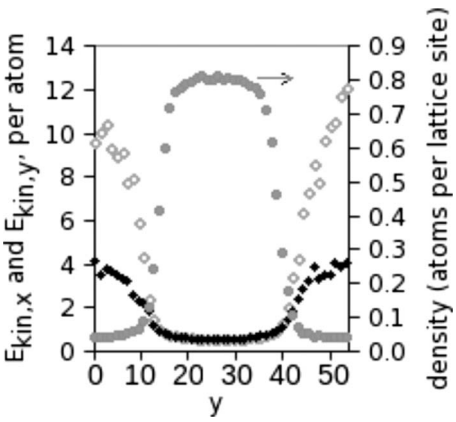


FIG. 8. Kinetic energy is inhomogeneous and anisotropic. $F_x=0.25$, $\lambda=1$, and $E_{kin}=0.7$. $E_{kin,x}$ (open diamonds) and $E_{kin,y}$ (filled diamonds) are on the left ordinate. Density (filled circles) is on the right ordinate. Energy is in units of $\epsilon$; $y$ is in units of $\sigma$.

Figure 9 shows the current density and particle density for the same conditions as in Fig. 8. Current is carried mainly by the low-density gas in the case shown. In off-lattice cases (i.e., with $\lambda=0$) the high-density region itself carries current by moving in the field direction as a unit.

The structure factor $S(k_x,k_y)$ was calculated from configurations and filed for analysis after the run. The structure factors parallel and perpendicular to the field, $S(k_x,0)$ and $S(0,k_y)$, were averaged over the structure factors collected during a run. Single-$k$ values $S(1,0)$ and $S(0,1)$ indicate anisotropy perpendicular and parallel to the field, respectively.

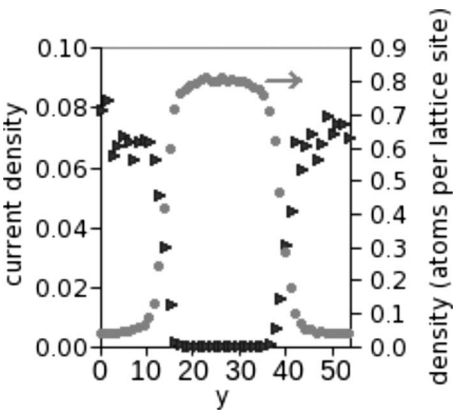


FIG. 9. $F_x=0.25$, $\lambda=1$, and $E_{kin}=0.7$. Current density (triangles) and particle density (circles) are shown. Current is carried mainly by low-density regions. Current density is in units of number of atoms per time per $\sigma$; $y$ has units of $\sigma$.

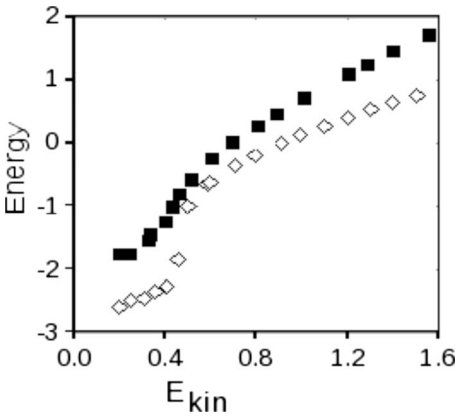


FIG. 10. Total energy as a function of kinetic energy for the equilibrium square-well system. For the upper data (filled squares), $\lambda=1$; on lattice. For the lower data (open diamonds), $\lambda=0$; off lattice. Energies are per atom and are in units of $\epsilon$.

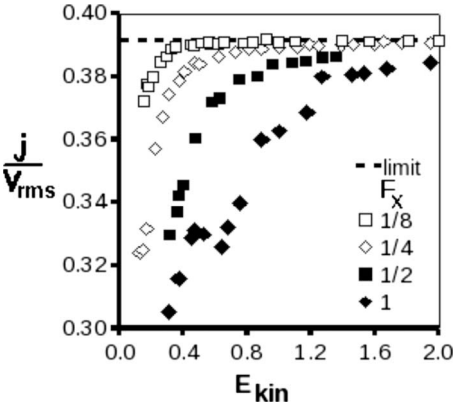


FIG. 11. Off-lattice current density, $j$, divided by root-mean-square velocity. Lattice strength $\lambda=0$. Driving field strength $F_x$: 1/8 (open squares, top curve), 1/4 (open diamonds), 1/2 (filled squares), and 1 (filled diamonds, bottom data). $E_{kin}$ is in units of $\epsilon$ per atom. $j/v_{rms}$ has units of number of atoms divided by $\sigma^2$.

## III. RESULTS

### A. Equilibrium square-well fluid

When the driving field $F_x=0$, steady state is the equilibrium state and average kinetic energy equals temperature. Equilibrium molecular-dynamics simulations were run with four values of $\lambda$: 0, 0.25, 0.5, and 1. Figure 10 shows the energy as a function of temperature for the gas off lattice, and on lattice with $\lambda=1$. In both cases and at the intermediate $F_x=0.25,0.5$ (not graphed) the only phase transition is solid-to-fluid. The nature of the low-temperature solid depends on the lattice strength, $\lambda$. Off lattice ($\lambda=0$) the solid is hexagonally close packed and isotropic, with enough defects to reduce the average number of bonds per particle, $N_{bonds}$, from 3 to 2.8. On lattice, the solid is a mixture of registered solids, $1\times1$, $2\times1$, and $3\times1$, plus regions of hexagonal packing. For $\lambda=1$ and 0.5, the solid consists mostly of $2\times1$ and $3\times1$ regions, and $N_{bonds}\approx2.4$. For $\lambda=0.25$, the solid is mostly hexagonal, resembling $\lambda=0$ configurations, and $N_{bonds}\approx2.7$. Based on the maximum in the heat capacity (not shown), the solid-fluid transition occurs at $E_{kin}\approx0.45$, independent of lattice strength. For comparison, phase transition in the lattice gas on a square lattice occurs at $T=2.269J/k\approx2.269\epsilon/(4k)=0.565$ in the present units.

In the special case $F_x=0$ and $\lambda=0$, the system reduces to the square-well fluid in two dimensions. The square-well system has been studied extensively in two and three dimensions. The equilibrium solid-liquid critical temperature for the present well width, $c=1.2449$, and in two dimensions, may be estimated from the $3d$ critical temperature $T_{C3D}=0.762$ [48] and the approximate ratio of the $d=2$ to $d=3$ critical temperatures, $T_{C2D}/T_{C3D}\approx0.66$ [49]: $T_{C2D}\approx0.762\times0.66=0.50$. The value 0.50 is not inconsistent with the phase transition temperature of approximately 0.45 indicated by the data in Fig. 10, considering that the molecular-dynamics simulation was not precisely at the off-lattice critical density and that no system-size corrections have been made.

### B. Driven off-lattice gas

Off lattice (i.e., with zero lattice potential, $\lambda=0$), for the field strengths used, current was observed even at the lowest kinetic energies simulated. Current density is proportional to the average $v_x$, and $v_x$ approaches the root-mean-square $v_{rms}$ at high kinetic energies, because the field biases velocity toward the $x$ direction $[v_{rms}=(2E_{kin})^{1/2}]$. Figure 11 shows $j/v_{rms}$ as a function of kinetic energy for various strengths of the driving field. The high-$E_{kin}$ limit is simply $N/\text{Area}$ which equals 0.392, because $N=1152$ and $\text{Area}=(24\times1.13\times2)^2$. Velocity anisotropy saturates at the limiting $j/v_{rms}$, where $\langle v_x\rangle\approx v_{rms}$. Figure 11 shows that increasing field strength *delays* saturation of velocity anisotropy to higher kinetic energy. In the absence of the lattice potential, there is evidently little resistance to flow.

The current density, under $F_x=1$, displays a break or dip at $E_{kin}\approx0.6$ in Fig. 11. The origin of that feature is unknown. It is not prominent in plots of $E_{pot}$, $N_{bonds}$, or structure factors.

At high kinetic energy, configurations showed a locally hexagonal solid, connected around large vacancies, and isotropic. Current came from the entire configuration being driven by the field.

Configurational relaxation was slow off lattice, at low kinetic energy, so reaching and identifying steady state was difficult. Under a weak field ($F_x=1/8$ and 1/4), below $E_{kin}=0.5$, multiple configurations appeared steady in the sense that no change in $N_{bonds}$ and $E_{pot}$ was apparent over $10^3$ time units. A single-strip configuration prepared with straight boundaries parallel to the field retained its shape and boundaries over $10^4$ time units. However, longer runs suggested that single-strip configurations having straight boundaries were unstable against break-up to isotropic configurations. Once the boundaries of a strip were perturbed, the strip did not reform. Also, such a strip was not observed to form from an initially random configuration. The present molecular-dynamics method poorly characterizes low-$E_{kin}$ off-lattice configurations under weak fields. Nonetheless, it can be concluded that low-field off-lattice systems show no evidence of stable anisotropic configurations, and boundaries of high-density regions are not preferentially oriented along the field.

At the highest field strength used, $F_x=1$, the structure factor reflects weak anisotropy parallel to and perpendicular to

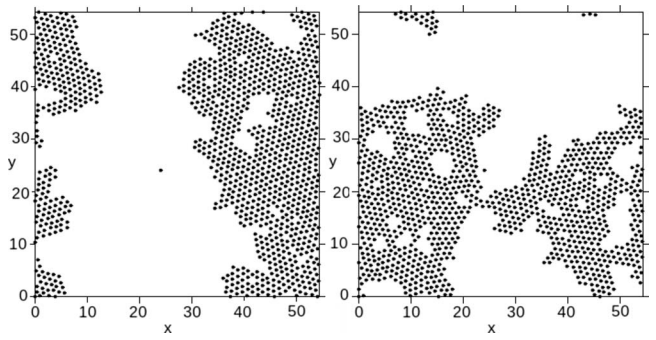


FIG. 12. Off-lattice configurations driven by $F_x=1$. The field direction is left to right. The left panel is a configuration from a steady state with $S(1,0)=290$, $E_{kin}=0.5$. The right panel is a configuration from a steady state with $S(0,1)=260$, $E_{kin}=1.9$. Coordinates $x$ and $y$ are in units of $\sigma$.

the field. Figure 12 shows configurations from the off-lattice system under field $F_x=1$. The configurations shown are from steady runs for which $S(0,1)$ was large (260), and for which $S(1,0)$ was large (380). Neither configuration, nor any other observed off lattice, approached the degree of anisotropic order observed on-lattice, e.g., Fig. 5(c), and in the driven lattice gas.

The configurations in Fig. 12 appear locally cold: high-density regions have local hexagonal order and boundaries relax only slowly. In an effort to quantify the apparent coldness, temperatures were calculated for the off-lattice systems in the following approximate way. The along-field velocity $v_x$ was averaged over configurations. Then temperatures parallel and perpendicular to the field were calculated relative to $\langle v_x \rangle$. $T_x=\langle \frac{1}{2}(v_x-\langle v_x \rangle)^2 \rangle$. $T_y=\langle \frac{1}{2}v_y^2 \rangle$. Figure 13 shows $T_x$ and $T_y$ for the off-lattice $F_x=1$ system. The calculated temperatures are lower than $E_{kin}$ and lower than the equilibrium freezing temperature. There is little temperature anisotropy, less than a factor of 2 between $T_x$ and $T_y$. It may be that interaction of the driving field, which continuously accelerates atoms along $x$, and the bath extracting heat, keeps the system's peculiar kinetic energy low. In some local equilibrium sense, the system is solid- or gel-like.

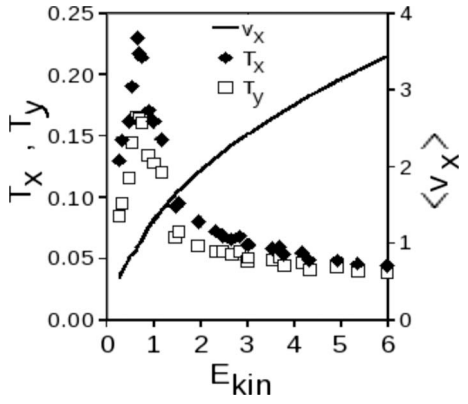


FIG. 13. Temperatures in the $x$ direction (solid diamonds) and $y$ direction (open squares) extracted from peculiar velocity under the field $F_x=1$. $\lambda=0$ (off lattice). The mean velocity in the field direction is the solid line. The unit of $E_{kin}$ is $\epsilon$, that of $T_x$ and $T_y$ is $\epsilon/k_B$, and $v_x$ has units of $\sigma$ divided by unitless time.

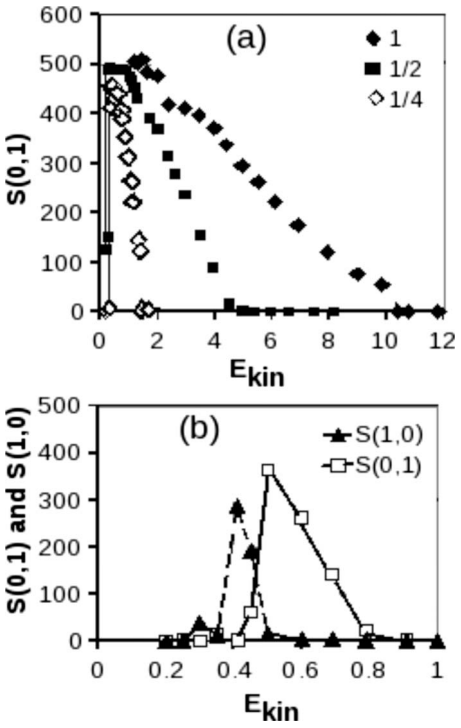


FIG. 14. Structure factors $S(0,1)$ and $S(1,0)$. Lattice strength $\lambda=1$. Upper graph (a): field strength $F_x=1$ (filled diamonds), 1/2 (filled squares), and 1/4 (open diamonds). Lower graph (b): field strength $F_x=1/8$. $S(0,1)$ (open squares), $S(1,0)$ (filled triangles). Lines are merely guides for the eyes. The structure factor is unitless. $E_{kin}$ is in units of $\epsilon$.

An underlying lattice potential sticks a frozen high-density slab in place, as indicated in Fig. 8 and discussed in Sec. II G. When the lattice potential is zero, as discussed in this section, the driving field pushes the configuration as a whole. The drifting configuration resembles the "flying ice cube" described by Harvey *et al.* [50]. The ice cube described by Harvey was an artifact of a molecular-dynamics heat bath that periodically rescaled velocity. It is not apparent that the present heat bath, as described in Sec. II C, would be subject to such an artifact. For the present model, off-lattice configurations are locally cold, drift under the field, and do not form ordered strips.

### C. Driven on-lattice gas

#### *1. Full-strength lattice,* $\lambda=1$

On the lattice, the field causes a high-density strip with edges parallel to the field direction. Examples are displayed in Figs. 5(b) and 5(c). These strips resemble those observed in the driven lattice gas. The structure factor $S(0,1)$ indicates single-strip anisotropy. As kinetic energy increases, $S(0,1)$ diminishes gradually, vanishing when the strip disappears into a homogeneous driven fluid. Under a weaker field, the one-strip configuration disappears at lower $E_{kin}$, under stronger field it persists to higher $E_{kin}$.

Figure 14 shows the structure factor $S(0,1)$ as a function of the kinetic energy per atom for four field strengths. For the lowest field strength, $S(1,0)$ is also shown. The arguments of

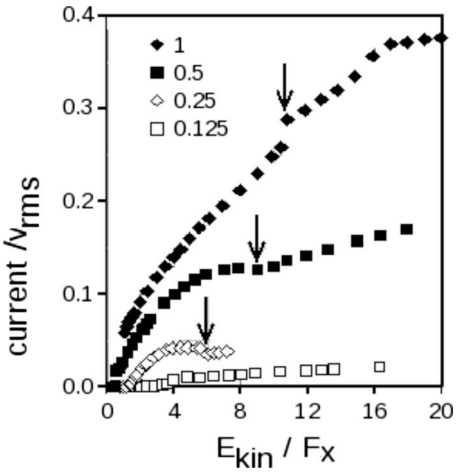


FIG. 15. On-lattice current density divided by root-mean-square velocity. Lattice strength $\lambda=1$. Driving field strength $F_x$: 1/8 (open squares), 1/4 (open diamonds), 1/2 (filled squares), and 1 (filled diamonds). On the abscissa, $E_{kin}$ is divided by $F_x$ merely to spread data that would otherwise be obscured near the origin. Current/$v_{rms}$ has units of number per $\sigma^2$. $E_{kin}/F_x$ has units of $\sigma$.

the structure factor are in units of the simulation length divided by $2\pi$, so $S(0,1)$ and $S(1,0)$ reflect a wavelength equal to the system size.

At the lowest field strength used, $F_x=1/8$, the structure factors graphed in Fig. 14 show that, as kinetic energy rises, the initially isotropic solid develops a rough strip *perpendicular* to the field, shown by the rise of $S(1,0)$. That anisotropy is replaced by a well-defined strip parallel to the field, as shown by the fall of $S(1,0)$ and subsequent rise of $S(0,1)$. The rise of $S(0,1)$ is due to a strip that resembles the DLG single-strip phase. It disappears to an isotropic fluid at $E_{kin} \approx 0.75$.

The solid appears to be isotropic at the lowest kinetic energies simulated. Current density, scaled by the root-mean-square speed, is graphed in Fig. 15 for four field strengths. At low kinetic energy the solid has zero or near-zero current. The onset of current corresponds with the initial rise in structure factor, in those cases in which a rise is visible. Extending simulations to lower kinetic energies would allow a better check of that concurrence, but slow relaxation prevented identification of steady states at lower kinetic energies.

The same anisotropic-to-isotropic transitions that are apparent in the structure factors are evident as dips or breaks in $j/v_{rms}$. The maximum possible value of $j/v_{rms}$, 0.392, is achieved when velocity is directed entirely along the field direction. Only the strongest field drives the system to near that limit. This is qualitatively different than on the zero-strength lattice, where even the weakest nonzero field, $F_x=0.125$, pushed $j/v_{rms}$ to its limit.

The potential energy per atom is graphed versus kinetic energy per atom in Fig. 16. Equilibrium energy (i.e., for $F_x=0$) is also shown. At a given total kinetic energy, driven systems have lower potential energy than the equilibrium system, mainly because in the driven system a larger number of attractive pair interactions contribute to lowering the potential energy. As the field diminishes, the potential energy of the driven system approaches that of the equilibrium system, as it must.

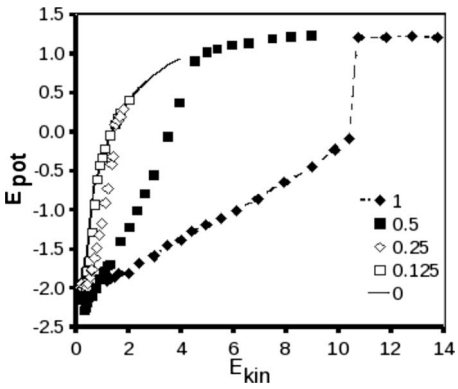


FIG. 16. Driven on-lattice potential energy versus average kinetic energy per particle. Lattice strength $\lambda=1$. Driving field strength $F_x$: 1/8 (open squares), 1/4 (open diamonds), 1/2 (filled squares), and 1 (filled diamonds). Equilibrium ($F_x=0$) is the solid line. Energies are in units of $\epsilon$. $F_x$ has units of $\epsilon/\sigma$.

### 2. *Half-strength lattice,* $\lambda=0.5$

As on the full-strength lattice, the low-temperature solid is isotropic and has near-zero current. Current rises when the structure factor rises, in the cases in which sufficiently low $E_{kin}$ values permit observation of the structure factor's rise from zero. A single-strip DLG-like anisotropic configuration breaks into an anisotropic fluid at high kinetic energy. As on the full-strength lattice, greater field strength moves the breakup to higher kinetic energy. Numerical results appear in Table I.

Also as on the full-strength lattice, at the lowest field strength $F_x=1/8$, rising $E_{kin}$ leads first to a rise in $S(1,0)$, an ordering perpendicular to the field, followed by a decline in $S(1,0)$ and a rise in $S(0,1)$. Qualitatively the same behavior is seen in Fig. 14(b).

## IV. CONCLUSIONS

The equilibrium case, $F_x=0$, of the present model system passes smoothly from a near-lattice system to a potential-free planar system. Trajectories on the strongest lattice potential, Fig. 5(a), resemble lattice-gas hopping. Melting is observed. The temperature or kinetic energy at which melting was observed did not depend strongly on lattice strength. Of course, more precise location of the transition, or a broader range of lattice strength, might reveal dependence on $\lambda$.

On lattice and driven, with $\lambda>0$ and $F_x>0$, the system behaves much like the driven lattice gas. Steady states in-

TABLE I. Kinetic energy at which isotropic fluid replaces the anisotropic strip.

| $F_x$ | $E_{kin}$ at $\lambda=0.5$ | $E_{kin}$ at $\lambda=1$ |
|---|---|---|
| 1/8 | 1.0 | 0.75 |
| 1/4 | 2.5 | 1.5 |
| 1/2 | 6.6 | 4.5 |
| 1 | No data | 10.5 |

clude DLG-like single-strip states, with the strips aligned with the field. The anisotropy is enhanced by larger field strength, as indicated by increasing $S(0,1)$ with increasing $F_x$, Fig. 14(a). At least at low field strengths, there is a threshold $E_{kin}$ below which the system is solid and does not carry current. Above that threshold, the field drives the system into an anisotropic current-carrying steady state, current increasing with $E_{kin}$. For low field strengths, structure factors indicate that the driven configurations order *perpendicular* to the field over a narrow range of $E_{kin}$, before forming a DLG-like strip along the field. Strips disappear into homogeneous fluid at transition kinetic energies that increase with increasing field strength, as in the DLG.

In the driven on-lattice system, current is carried primarily by the low-density gaslike region. This is in contrast to the DLG and the off-lattice driven Lennard-Jones fluid (DLJF), both of which are Monte Carlo models. In the DLG, current is carried equally by the high- and low-density regions. In the off-lattice DLJF, most current is carried by the high-density region. In both the DLG and the DLJF, the largest current density is at the interface between high- and low-density regions [51,52]. The origin of the current-carrying difference between the present model and the Monte Carlo models may arise from temperature. Temperature is a homogeneous and isotropic parameter in customary Monte Carlo rates. In the present MD model, kinetic energy is inhomogeneous and anisotropic. To the extent that $E_{kin}$ represents temperature, low-density regions are hotter and so more conductive than high-density regions, as indicated by Fig. 8, for example.

When off lattice (i.e., with $\lambda=0$) the present MD model is unlike the driven lattice gas in the sense that its configurations are approximately isotropic, solidlike with large vacancies. No single-strip ordered states appeared to the largest field strengths and kinetic energies simulated. Of course, larger fields and energies might yield other behavior. Observed particle current was large down to the lowest kinetic energies that were reached in the simulations. At higher $E_{kin}$, current closely approached the root-mean-square-speed limit, for the four values of $F_x$ used in the simulations, as shown in Fig. 11. The on-lattice MD model resembles the DLG because the lattice mixes flow, scattering velocities at each impact. That imparts Markov-type properties to the dynamics, as in a Monte Carlo lattice model. Off lattice, only particle-particle collisions are left to fulfill that role, and their effect is suppressed by streaming along the field.

Temperature, in concept and in calculation, is a problem for this and other nonequilibrium molecular-dynamics models. In the present work, kinetic energy was used as an organizing and control parameter. It may not be ideal for the purpose. As Baranyai [37] remarked, "It seems very likely that the kinetic temperature of [*nonequilibrium molecular-dynamics*] models is a wrong candidate for the role one can expect from a temperature-like quantity." Although kinetic energy is a readily calculated and well-defined proxy for temperature, it is not entirely satisfactory for organizing steady-state properties.

A natural strength of the molecular-dynamics method is its ability to calculate time-dependent properties. Relaxation dynamics can be studied. Also, time reversal is available so irreversibility and entropy production may be accessible in future work. Those strengths of molecular dynamics were not realized in the present work, which focused on characterizing steady states, but should be in future work.

## ACKNOWLEDGMENTS

This research was supported in part by the National Science Foundation through TeraGrid resources provided by Oak Ridge National Laboratory (ORNL), Purdue University (steele), and the University of Chicago and Argonne National Laboratory (UC/ANL). This work also relied upon computer access granted by the Minnesota Supercomputing Institute of the University of Minnesota. Additional computing resources were provided by the Department of Chemistry and Biochemistry of the University of Minnesota Duluth.

[1] W. Strepp, S. Sengupta, and P. Nielaba, Phys. Rev. E **63**, 046106 (2001).
[2] W. Strepp, S. Sengupta, and P. Nielaba, Phys. Rev. E **66**, 056109 (2002).
[3] P. Chaudhuri, C. Das, C. Dasgupta, H. R. Krishnamurthy, and A. K. Sood, Phys. Rev. E **72**, 061404 (2005).
[4] P. T. Korda, G. C. Spalding, and D. G. Grier, Phys. Rev. B **66**, 024504 (2002).
[5] F. Q. Potiguar and R. Dickman, Phys. Rev. E **76**, 031103 (2007).
[6] A. M. Lacasta, J. M. Sancho, A. H. Romero, and K. Lindenberg, Phys. Rev. Lett. **94**, 160601 (2005).
[7] J. Marro, P. L. Garrido, and M. Díez-Minguito, Phys. Rev. B **73**, 184115 (2006).
[8] J. Marro, Comput. Phys. Commun. **179**, 144 (2008).
[9] M. Díez-Minguito, P. L. Garrido, and J. Marro, Phys. Rev. E **72**, 026103 (2005).
[10] P. D. Siders, J. Stat. Phys. **119**, 861 (2005).
[11] S. Katz, J. L. Lebowitz, and H. Spohn, Phys. Rev. B **28**, 1655 (1983).
[12] S. Katz, J. L. Lebowitz, and H. Spohn, J. Stat. Phys. **34**, 497 (1984).
[13] N. C. Pesheva, Y. Shnidman, and R. K. P. Zia, J. Stat. Phys. **70**, 737 (1993).
[14] B. Schmittmann and R. K. P. Zia, *Statistical Mechanics of Driven Diffusive Systems*, Phase Transitions and Critical Phenomena Vol. 17 (Academic Press Limited, London, 1995).
[15] R. Dickman, Phys. Rev. A **38**, 2588 (1988).
[16] J. Marro and R. Dickman, *Nonequilibrium Phase Transitions in Lattice Models* (Cambridge University Press, Cambridge, 1999).
[17] H. K. Janssen and B. Schmittmann, Z. Phys. B **64**, 503 (1986).
[18] K. Leung and J. L. Cardy, J. Stat. Phys. **44**, 567 (1986).
[19] K. T. Leung, Phys. Rev. Lett. **66**, 453 (1991).

[20] P. L. Garrido, M. A. Muñoz, and F. de los Santos, Phys. Rev. E **61**, R4683 (2000).
[21] F. de los Santos, P. L. Garrido, and M. A. Muñoz, Physica A **296**, 364 (2001).
[22] S. Caracciolo, A. Gambassi, M. Gubinelli, and A. Pelissetto, J. Stat. Phys. **115**, 281 (2004).
[23] R. Lefevere and H. Tasaki, Phys. Rev. Lett. **94**, 200601 (2005).
[24] M. Q. Zhang, Phys. Rev. A **35**, 2266 (1987).
[25] Q. Zhang, Ph.D. thesis, Rutgers, the State University of New Jersey, Rutgers, New Jersey, 1987.
[26] K. S. C. Kumaran, Master thesis, University of Minnesota Duluth, Duluth, Minnesota, 2004.
[27] D. Frenkel and B. Smit, *Understanding Molecular Simulation From Algorithms to Applications*, Computational Science From Theory to Applications Vol. 1, 2nd ed. (Academic Press, San Diego, 2002).
[28] D. A. Young and B. J. Alder, J. Chem. Phys. **73**, 2430 (1980).
[29] S. B. Kiselev, J. F. Ely, and J. R. Elliott, Jr., Mol. Phys. **104**, 2545 (2006).
[30] J. K. Singh and S. K. Kwak, J. Chem. Phys. **126**, 024702 (2007).
[31] A. Skibinsky, S. V. Buldyrev, A. Scala, S. Havlin, and H. E. Stanley, Phys. Rev. E **60**, 2664 (1999).
[32] P. Bolhuis, M. Hagen, and D. Frenkel, Phys. Rev. E **50**, 4880 (1994).
[33] J. P. J. Michels and N. J. Trappeniers, Physica **101A**, 156 (1980).
[34] W. Kwak, D. P. Landau, and B. Schmittmann, Phys. Rev. E **69**, 066134 (2004).
[35] J. Casas-Vazquez and D. Jou, Phys. Rev. E **49**, 1040 (1994).
[36] G. P. Morriss and L. Rondoni, Phys. Rev. E **59**, R5 (1999).
[37] A. Baranyai, Phys. Rev. E **61**, R3306 (2000).
[38] A. Baranyai, Phys. Rev. E **62**, 5989 (2000).
[39] O. G. Jepps, G. Ayton, and D. J. Evans, Phys. Rev. E **62**, 4757 (2000).
[40] W. G. Hoover and C. G. Hoover, Phys. Rev. E **77**, 041104 (2008).
[41] E. G. D. Cohen, J. Stat. Mech. Theor. Exp. (2008) P07014.
[42] M. P. Allen and D. J. Tildesley, *Computer Simulation of Liquids* (Oxford University Press, Oxford, 1987), Chap. 7.
[43] B. D. Todd and P. J. Daivis, Mol. Simul. **33**, 189 (2007).
[44] J. Delhommelle, J. Petravic, and D. J. Evans, Phys. Rev. E **68**, 031201 (2003).
[45] J. Delhommelle, Phys. Rev. E **71**, 016705 (2005).
[46] D. C. Rapaport, *The Art of Molecular Dynamics Simulation*, 2nd ed. (Cambridge University Press, Cambridge, 2004).
[47] B. J. Alder and T. E. Wainright, J. Chem. Phys. **31**, 459 (1959); Eqs. Ia1 and 2b contain minor typographical errors.
[48] F. Del Río, E. Ávalos, R. Espíndola, L. F. Rull, G. Jackson, and S. Lago, Mol. Phys. **100**, 2531 (2002).
[49] F. Del Río and A. G. Villegas, J. Phys. Chem. **95**, 787 (1991).
[50] S. C. Harvey, R. K. Tan, and T. E. Cheatham III, J. Comput. Chem. **19**, 726 (1998).
[51] M. Díez-Minguito, P. L. Garrido, and J. Marro, *Lattice versus Lennard-Jones Models with a Net Particle Flow*, Traffic and Granular Flow 05, edited by A. Schadschneider and T. Pöschel (Springer, Berlin, 2007), pp. 53–62; Figure 4 shows current profiles.
[52] M. D. Minguito, Ph.D. thesis, Universidad de Granada, 2007; current profile is in Fig. 4.8.